ACS Photonics

Article

pubs.acs.org/journal/apchd5

Zinc Oxide Based Plasmonic Multilayer Resonator: Localized and Gap Surface Plasmon in the Infrared

Jongbum Kim,[†] Aveek Dutta,[†] Babak Memarzadeh,[‡] Alexander V. Kildishev,[†] Hossein Mosallaei,[‡] and Alexandra Boltasseva*[,†]

[†]Birck Nanotechnology center and School of Electrical & Computer Engineering, Purdue University, West Lafayette, Indiana 47907, United States

[‡]Department of Electrical and Computer Engineering, Northeastern University, Boston, Massachusetts 02115, United States

Supporting Information

ABSTRACT: Using alternative plasmonic materials, we experimentally demonstrate gap plasmon resonances in metal−insulator−metal nanostructures in the near- and mid-infrared wavelength regions utilizing gallium doped zinc oxide as the metallic component and undoped zinc oxide as the dielectric. We show that similar to metal−insulator−metal resonators previously demonstrated with noble metals, the layered transparent conducting oxide nanodisks support gap surface plasmon resonances characterized by highly confined electromagnetic fields in the dielectric gap. Such resonances can be tailored to desired values by varying the dielectric-layer thickness. Utilizing these observed gap plasmon resonance, we examine the potential of our structure for sensing applications by measuring the surface enhanced infrared absorption of an octadecanethiol layer. The layered nanostructure can detect very weak absorption resonances in nanoscale volumes of absorbing material deposited over the nanodisk resonator.

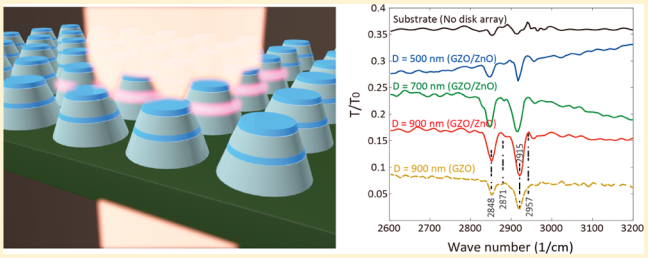

KEYWORDS: *transparent conducting oxide, plasmonics, surface plasmon polariton, surface plasmon resonance, semiconductor, infrared sensing*

Subwavelength metallic nanostructures are capable of supporting localized surface plasmon resonances (SPRs), which are collective oscillations of the surface conduction electrons excited by electromagnetic (EM) waves in the optical range.[1] The unique features of SPRs have attracted great interest because of their potential applications in chemical and biological sensors,[2−4] surface enhanced spectroscopy,[5−7] integrated optical circuits,[8,9] and nanoscale optical devices.[10,11] The frequency range and position of the resonance depends on the geometry and optical properties of the constituent materials; therefore, the material and the geometry should be considerately designed to achieve the required functionality. To date, gold (Au) and silver (Ag) have been used for the majority of the experimental work and demonstrations due to their abundance of free electrons which enable plasmonic resonance in the visible range. However, high optical losses in the infrared (IR) range have prevented some of the more promising applications from being realized.[12−15] Additionally, these noble metals have other drawbacks, such as difficulty in fabricating nanostructures, incompatibility with well-established processes for silicon based products, and lack of tunability. With the demand of alternative materials to extend the range of applications, transparent conducting oxides (TCOs) have been proposed as a promising new class of plasmonic materials for the telecom and IR applications.[16−19]

Advantages of TCOs over noble metals include compatibility with conventional fabrication techniques, tunable optical properties, chemical and mechanical stabilities, and low intrinsic optical losses due to the wide band gap and small Drude damping (γ). The recent emergence of alternative plasmonic materials has led to the demonstration of TCO-based resonant devices such as synthesized nanospheres,[20−23] self-assembled standing nanorods,[24,25] and lithographically patterned nanodisk[26] and nanorod metasurfaces.[27] These works have shown that TCOs can provide unprecedented capabilities as an alternative to metal for resonant application in the IR spectral range. However, despite investigations of various geometries of TCO nanostructures, no attention has been paid to the multilayer metal/dielectric geometry with TCOs as the metallic component. Conventionally, metal−insulator−metal (MIM) configurations have been extensively studied for negative index metamaterials (NIMs) due to their magnetic resonance and local field confinement in the insulator region, which are referred to as gap surface plasmon (GSP) resonance.

In this work, we experimentally realize a four-layer nanodisk resonator consisting of alternating layers of zinc oxide (ZnO) and gallium doped ZnO (GZO), as shown in Figure 1. We

Received: June 5, 2015
Published: July 28, 2015

DOI: 10.1021/acsphotonics.5b00318
ACS Photonics 2015, 2, 1224−1230

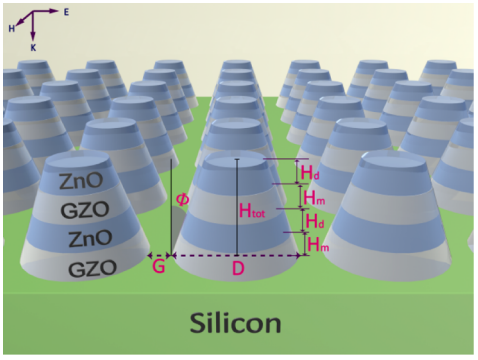

Figure 1. Schematic view of an array of multilayer transparent conducting oxide nanodisk resonators and the definition of the relevant parameters. Gallium-doped zinc oxide (GZO) serves as the metallic component, while ZnO serves as the dielectric spacer layer. G is the separation between adjacent nanodisks, φ is the angle of the side wall of the nanodisk, and D is the disk size. H_{tot} is the total thickness of multilayer nanodisk, and H_d and H_m are thickness of individual ZnO and GZO, respectively.

study and quantify the performance of TCO-based layered nanostructures and provide guidance for designing IR plasmonic devices with highly doped oxide semiconductors for sensing and beam steering applications as well as optical waveguides. As a potential applications of TCO-based MIM resonators, we demonstrate surface enhanced infrared absorption (SEIRA) used extensively in biospectroscopy. The strongly localized electromagnetic fields at metallic nanostructures enhance the absorption from vibrational and rotational modes of nearby bio molecules making TCO nanostructures a promising candidate for IR sensing applications.

SAMPLE PREPARATION AND CHARACTERIZATION

In contrast with Ag or Au, one of the most important advantages of TCOs is that its intrinsic optical properties can be adjusted and tailored. The adjustability of the optical properties is achieved by altering the carrier density and electron mobility by controlling the doping rate and introducing compositional defects.[12] Controlling the deposition parameters provides a simple method to realize nanostructures of alternating metal and dielectric layers using TCOs. ZnO is a native n-type doped semiconductor with carrier concentrations of 10^{16} cm^{-3}, thus, functioning as a dielectric below wavelengths of 8 μm.[28] However, if the carrier concentration is dramatically increased up to 10 ^{21} cm^{-3} with 6 wt % doping of gallium, GZO will have metal-like behavior in the NIR.[29] Due to these properties, for operating in the IR, we can construct a multilayer configuration of nanodisks with GZO as the metallic components and ZnO as the dielectric component.

By employing conventional lift-off process as reported in our previous work,[26] we fabricate GZO/ZnO multilayer nanodisk resonators. By rotating the target in the PLD system during deposition, four layers consisting of alternating GZO ZnO layers were deposited and the number of laser pulses for each target was calculated to achieve the desired thickness. The total thickness (T_{tot}) of each multilayer nanodisk is 320 nm, with adjacent nanodisks spaced 100 nm apart in a 2-D array; furthermore, the diameter (D) is varied from 500 to 900 nm. The scanning electron microscope (SEM) image in Figure 2a shows the nanopatterned multilayer nanodisk array. It is notable that the TCO nanodisk fabricated by lift-off process produces nonvertical side walls, hence the vertical cross-section of the nanodisk presents a trapezoidal shape (Figure 2b). Since both GZO and ZnO are conductive, two materials cannot be distinguished in the SEM image. To image the multilayer configuration of the nanodisk, high-angle annular dark-field imaging (HAADF) scanning transmission electron microscope (STEM) along with energy dispersive X-ray spectroscopy (EDS) was used. This method is highly sensitive to variations in the atomic number of atoms in the sample. Therefore, it is suitable to detect the Ga and Zinc atom concentrations, which have atomic number of 30 and 31, respectively.[30] A silicon oxide (SiO_2) layer was deposited on top of the nanodisks to protect the sample while milling with focus ion beam (FIB) of Gallium for EDS characterization. The K-line X-ray is used to scan the sample and the energy resolution is 0.7 eV (see Supporting Information, Figure S1, for EDS spectrum of cross-section of multilayer nanodisk). Figure 2b shows an SEM cross-section image of two milled multilayer nanodisks. The EDS scanning area is marked with a red, square line in Figure 2b. The height and length of the scanned image is 336 nm with 64 pixels. The EDX elemental maps for zinc, gallium, and silicon, obtained by integration of the element's background-subtracted K-line X-ray peak, show that multilayer nanodisk are comprised of a zinc layered with gallium, as expected. The presence of

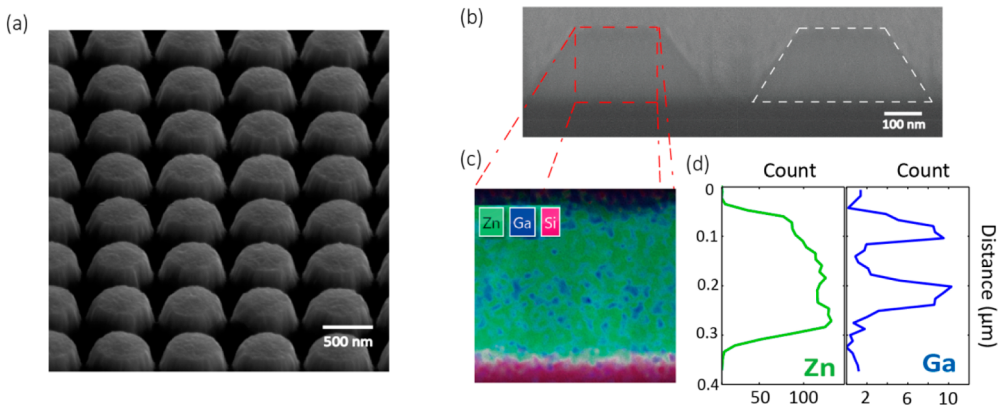

Figure 2. (a) Tilted SEM image (52°) of an array of GZO nanodisks with a mean diameter D = 700 nm, height H_{tot} = 320 nm, and gap between two disks G = 100 nm. (b) Tilted SEM cross-section image (80°) of nanodisks at high magnification. The energy dispersive X-ray spectroscopy (EDS) mapping area is marked with dashed red line. (c) EDS mapping of elements zinc, gallium, and silicon of a multilayer nanodisk. (d) The line scan of Zn and Ga across the nanodisk.

DOI: 10.1021/acsphotonics.5b00318
ACS Photonics 2015, 2, 1224−1230

gallium ions identified throughout the EDS sample is indicative of the contamination due to gallium ion milling. Nevertheless, the GZO layers still contain relatively large Ga concentration, and the two layers of GZO are clearly observed in the line scan plotted in Figure 2 d. The EDS line scan along the multilayer nanodisk quantifies the doping level of gallium to the sum of zinc and gallium as 6 wt %.

The optical properties of the GZO and ZnO films were characterized by variable angle spectroscopic ellipsometry (V-VASE, J. A. Woollam) in the spectral region from 350 to 2500 nm. The dielectric function of the film was retrieved by fitting a Drude + Lorentz oscillator model to the ellipsometry data. In semiconductors, conduction electrons have a nearly continuum of available states, so that their interaction with an electromagnetic field is well approximated by Drude theory where conduction electrons are treated as a three-dimensional free-electron gas. The Lorentz oscillator model is used to describe the absorption of photons by valence electrons. The following eq 1 describes the Drude + Lorentz oscillator model where the second term comes from the Drude model and the third term represents the Lorentz oscillator.

$$\varepsilon(\omega) = \varepsilon_\infty - \frac{\omega_p^2}{\omega(\omega + i\Gamma_p)} + \frac{f_l \omega_l^2}{\omega_l^2 - \omega^2 - i\omega\Gamma_l} \quad (1)$$

Here ε_∞ is the background permittivity, ω_p is the unscreened plasma frequency, Γ_p is the carrier relaxation rate, and f_l is the strength of the Lorentz oscillator with center frequency ω_l and damping Γ_l. Our model used to fit the ellipsometry data consisted of a four-layered structure with the ZnO permittivity assumed to be equal to the permittivity of 70 nm thick ZnO films deposited under identical conditions. We choose the GZO thickness as a free parameter in our fitting model and found the fitted thickness to deviate from the thickness characterized by EDS to be 4 nm. In Figure 3, we plot the dielectric functions of ZnO and GZO thin films extracted from Drude + Lorentz oscillator parameters from 1 to 7 μm. It has been reported that the dielectric function of doped ZnO are dominated by Drude-Lorentz oscillator model up to around 70 μm where the additional resonance originated from the ZnO phonon resonance limits the fitting of these oscillators to retrieve dielectric function of doped ZnO.[31] Therefore, we retrieved the optical properties of GZO and ZnO film in the spectral region from 350 nm to 2.5 μm and calculated those properties from 2.5 to 7 μm with the extracted Drude-Lorentz model parameters. As shown in Figure 3, the optical properties of GZO have a strong dependence on the thickness of the film's thickness. We believe that this difference for different thickness of GZO films is caused by the interface with the substrate, which can have many carrier trap states reducing the net carrier concentration. However, when GZO thin films are grown between ZnO layers without breaking the vacuum, the crystallinity of polycrystalline GZO thin films can be preserved because of proper lattice matching and growth orientation between GZO and ZnO. The ZnO layer helps to cure the trap states at the interface, resulting in the optical properties of the 70 nm GZO film sandwiched between ZnO to be similar to that of the 320 nm thick GZO film. Therefore, in spite of reducing the thickness of the GZO layer, we can maintain the optical properties of the GZO films in layered geometries by using ZnO as a dielectric layer.

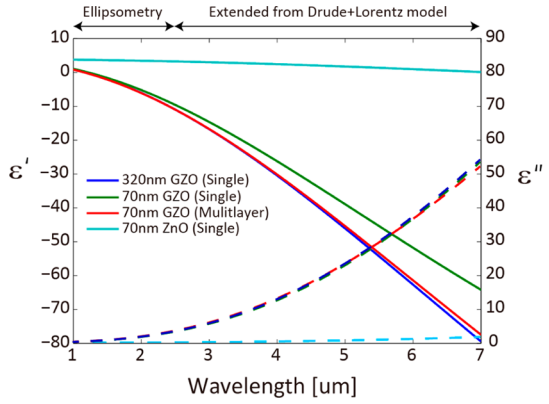

Figure 3. Real (solid line) and imaginary (dashed line) parts of the dielectric function of ZnO thin films and GZO thin films. Multilayer indicates that GZO film is sandwiched with ZnO films.

RESULTS AND DISCUSSION

We fabricated the multilayer ZnO/GZO nanodisk array consisting of 40 nm thick ZnO and 120 nm thick GZO; therefore, the dielectric (ZnO) to metallic (GZO) ratio is 1:3. We also prepared GZO nanodisks without intermediate ZnO layers (i.e., pure GZO nanodisks) to observe the influence of the dielectric layers. The overall dimension of the single-layer GZO nanodisk array (H_{tot} = 320 nm and G = 100 nm) is the same as the multilayer nanodisk array. The transmission spectra were obtained using a Fourier Transform Infrared Spectroscopy (FTIR) with 0.52 numerical aperture (NA). The measurement is performed in the wavelength range from 1.5 to 7 μm due to the absorption from silicon substrate in visible range. Figure 4 shows the transmission of the GZO nanodisk array and ZnO/GZO multilayer nanodisk array. For GZO nanodisks, two strong resonances (dips) are detected at the near-infrared (NIR) and the mid-infrared (MIR). However, multilayer nanodisks have three transmission resonances (dips) at 1.8, 3.0, and 5.2 μm wavelengths. To gain insight into the characteristic of the transmission resonances for both single-layer and multilayer nanodisk arrays, the experimental spectra are verified by simulations with Finite Element Method (FEM) based commercial software, Comsol Multiphysics. The optical properties of GZO thin film extracted from ellipsometry measurement are used for modeling of nanodisk array. Overall, the resonance dips in transmission are weaker in experiments than in simulations. This is consistent with the inevitable imperfections in nanofabrication processes, which lead to surface roughness and so on. In addition, the properties of patterned TCOs change when compared to the properties of thin continuous films since nanostructuring introduces more surface area with surface traps/states that change the carrier concentration.

We first explore the resonances in a single-layer nanodisk by mapping the near-field distribution at the wavelengths of 1.7 μm (I) and 4.2 μm (II), where the two strong dips are observed. At the 1.7 μm NIR dip, the electric field is localized and distributed across the top surface of the nanodisk and peaks at the corners, as shown in Figure 5a. Considering the fact that the LSPR field decays rapidly away from the surface, the field profile at the wavelength of 1.7 μm implies a LSPR at the surface of the nanodisk. In contrast to the near-field distribution at resonance (I), the E-field profile at 4.2 μm shows the field enhancement on the edge at the nanodisk boundary and a weak field at the top edge of the nanodisk. As depicted in Figure 5b,

DOI: 10.1021/acsphotonics.5b00318
ACS Photonics 2015, 2, 1224−1230

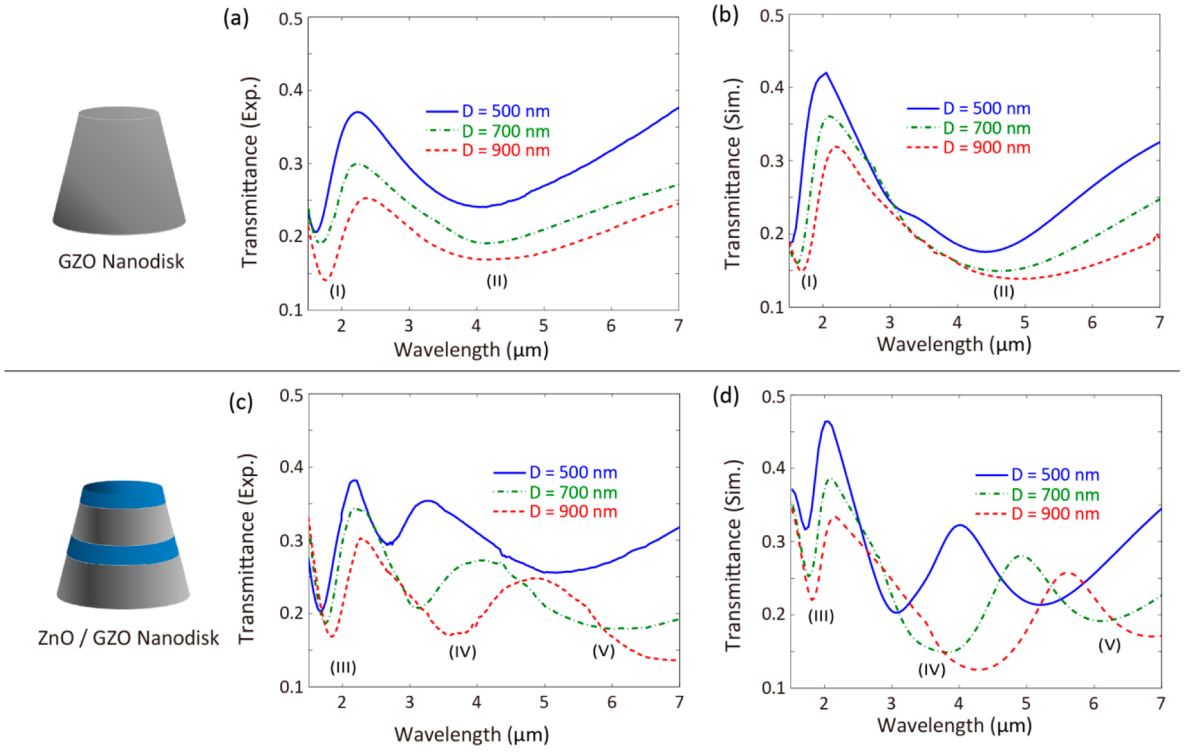

Figure 4. Transmission spectra of single-layer GZO nanodisk resonators ((a) experiment, (b) simulation) and multilayer GZO/ZnO nanodisk resonators ((c) experiment, (d) simulation) with different disk diameters.

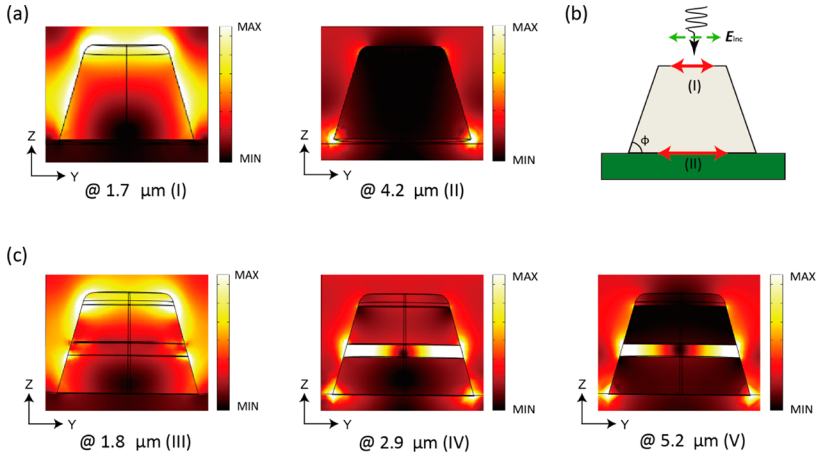

Figure 5. (a) Cross-sectional and top view of near-field distribution of the GZO nanodisk (h = 320 nm, d = 500 nm, g = 100 nm) at the wavelengths of interests ((I) and (II) in Figure 4). (b) Schematic view of the interaction between nanodisk and incident light, two resonance mode can be excited due to the side-wall angle. (c) Cross-sectional and top view of the near-field distribution of the ZnO/GZO nanodisk (h = 320 nm, d = 500 nm, g = 100 nm, h_d = 40 nm, h_m = 120 nm) at the wavelength of interests ((III), (IV), and (V) in Figure 4).

the incident wave can be coupled at the two interfaces (I) and (II) (see Supporting Information, Figure S1, for additional numerical simulation results on geometrical consideration of GZO nanodisks). Due to the large refractive index of the silicon substrate (n = 3.44) compared to air (n = 1), the EM near-field resonance of the nanodisk is broken in two, shifting a large portion of such field toward the substrate at the MIR resonance. While for NIR resonance (I) it can be noted that the EM near-field is mostly localized at the periphery of the top surface without interacting with the substrate. Qualitatively, if we consider a spherical lossless Mie scattering particle, this condition can be expressed as $2\varepsilon_{GZO} = \varepsilon_d$, where ε_{GZO} and ε_d describe the real part of the dielectric function of GZO and surrounding media, respectively. The dispersion of ε_{GZO} and the difference between the permittivity of air (ε_{air}) and silicon (ε_{Si}) lead to the remarkable shift of resonance position.

As the disk diameter increases, the resonance (I) is red-shifted and becomes stronger. This is due to the fact that the disks begin to support higher order plasmonic modes that start to overlap as the disk size increases.[32,33] Similarly, the MIR resonance wavelength (II) is also red-shifted while increasing the disk size. In fact, the resonance redshift with increasing the disk size has been observed in noble metal nanoparticles in the visible region, suggesting that the plasmonic properties and tendency of TCO-based nanostructure can be estimated by the

DOI: 10.1021/acsphotonics.5b00318
ACS Photonics 2015, 2, 1224−1230

general plasmonic properties of nanostructures with conventional metal in a different wavelength domain.

Based on the understanding of the resonance characteristic of GZO nanodisks, we analyze the resonance properties of multilayer nanodisks with a similar method. Considering the field distribution of multilayer nanodisk at the wavelength of 1.8 μm, as shown in Figure 5c, the resonance in NIR (III) corresponds to the LSPR of two GZO layers separated with ZnO. This spectral feature is quite similar to the LSPR of GZO nanodisks. For the resonance (IV) at the 3.0 μm wavelength, one can see that the field is obviously enhanced inside the dielectric layer. Such high field enhancement inside the dielectric layer of MIM structure is attributed to the GSP, which are propagating surface plasmon polaritons (SPPs) at the interface between metal and dielectric, observed in noble metal based MIM geometry in the visible range.[34−36] Owing to the interaction of the SPPs at the two interfaces between GZO and ZnO, SPPs are slowed down and the slow-light SPP coupled into the ZnO regime forms a standing-wave resonance under the condition of constructive interference, leading to the enhanced light-matter interaction.[34,37] The resonance wavelengths (λ) have to satisfy the Febry-Perot equation, as reported in the theoretical study:[38]

$$w\frac{2\pi}{\lambda}n_{pp} = m\pi - \varphi \quad (2)$$

where w is the width of the resonator, $n_{pp} = \mathrm{Re}(\beta/k_0)$ is the real part of the mode-index of the GSP, φ is the reflection phase, and m is an integer referring to the order of the resonance.[39] The dependence of resonance wavelength on disk size is clear evidence that the identified resonance are caused by GSP. From the equation, we can notice that the resonance wavelength is linearly shifted with increasing resonator width. It is well-matched with the experimental result on variation of resonance wavelength with regard to the increase of disk size.

The mismatch of magnitude of transmission spectra at 3.0 μm wavelength is ascribed to the surface roughness of side wall, which can increase the scattering of light at the boundary of dielectric layer and reflected SPPs at the end of ZnO layer is reduced. Furthermore, additional intrinsic optical loss of GZO nanodisk can arise from nanopatterning of GZO layers.[36,40] For the resonance at the wavelength of 5.2 μm, similar to the resonance properties of single-layer GZO nanodisk, lights gets trapped at the boundary between the nanodisk and the substrate. Notably, the multilayer GZO nanodisk sustained the two LSPRs excited in the single-layered GZO nanodisk despite the introduction of dielectric layers.

By varying the portion of dielectric layer in multilayer nanodisk, we explore the tunability of three different types of resonances ((III), (IV), and (V) in Figure 4). Figure 6 shows the resonance frequencies in multilayer GZO/ZnO nanodisk as a function of the ratio of the dielectric layer. Since T_{tot} is constant (320 nm), the thickness of GZO and ZnO layers simultaneously change as the ratios are varied. For instance, 50% of ZnO means that the thickness of the GZO and ZnO layers are 80 and 80 nm, respectively. The resonances of multilayer nanodisks shift toward longer wavelength by increasing the proportion of dielectric. The variations of resonance wavelength of two LSPR ((III) and (IV)) are determined by the modified effective permittivity of layered configuration. With manipulation of dielectric thickness, the effective permittivity of the nanodisk can be engineered as we desire. TCOs have small magnitude and weak dispersion of real

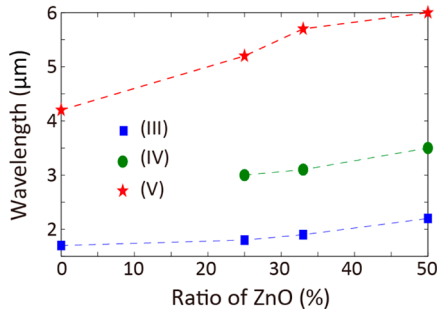

Figure 6. Resonance wavelength of multilayer nanodisk resonators with different thickness ratio between ZnO and GZO as a function of percentage of ZnO.

part of permittivity compared to noble metal; therefore, tunability of resonance wavelength is significant by controlling the dielectric thickness. It should be noted that the tunability of GSP resonance (II) is ascribed the change of effective index of SPP mode at the interface of metal and dielectric.[37] GSP is also easily controlled by modifying the nanostructure dimensions and the dielectric-layer thickness. Building a multilayer geometry is the efficient and feasible approach to engineering the resonance properties of plasmonic nanostructures without changing the properties of the materials.

Finally, we characterize the capability of multilayer nanodisk arrays for mid-infrared SEIRA. To date, most SEIRA-based applications have been demonstrated using resonant nanostructures consisting of noble metals such as Ag and Au; however, we believe noble metals to be a limited material platform. In contrast, our materials surpass noble metals in terms of tunability, compatibility with other materials, and simplicity of geometry to create resonance in the IR range. For the characterization of SEIRA of GZO/ZnO nanodisk resonator, the layered nanodisk with the ratio of 1:3 between ZnO and GZO is covered with an octadecanethiol ($C_{18}H_{37}SH$) layer. The dominant absorption from vibrational modes of octadecanethiol (ODT) molecules are located very close to the GSP resonance of the multilayer nanodisk.[41] To cover the nanodisk with an ODT layer, the sample was exposed to 1 mM solution of ODT in ethanol during 24 h; the samples were then taken out of the ODT solution, thoroughly rinsed with ethanol to remove any excess amount of unbound ODT molecules, and dried with nitrogen gas. SEM images in the Figure 7a shows the formation of ODT layers on top of nanodisks.[42] The ODT layer is randomly aggregated during solvent evaporation, but the thickness of the layer is, on average, around 20 nm and the coverage over the entire array is 70%.

IR spectra were obtained with FTIR spectrometer and normalized with transmission of multilayer nanodisk without ODT layer, as shown in Figure 7b. The reference spectrum also was taken from a bare silicon substrate. From the measurements, distinguishable absorption peaks of ODT molecules assigned from CH stretching vibrations are as follows: symmetric CH_2 stretch (2848 cm^{-1}), symmetric CH_3 stretch (2871 cm^{-1}), antisymmetric CH_2 stretch (2915 cm^{-1}), and antisymmetric CH_3 stretch (2957 cm^{-1}).[41] Even though the aggregated ODT layer makes it difficult to directly compare between spectrum from bare silicon substrate and from multilayer nanodisk, it is noted that the absorption spectrum of ODT molecules become stronger as the GSP resonances are well-aligned with the ODT absorption spectral lines. For example, we are able to clearly detect the very weak ODT

DOI: 10.1021/acsphotonics.5b00318
ACS Photonics 2015, 2, 1224−1230

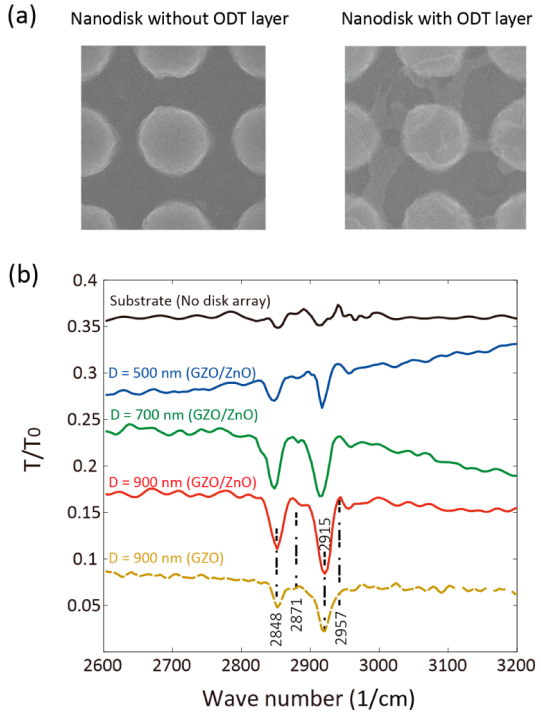

Figure 7. (a) SEM images of multilayer nanodisk array without (left) and with octadecanethiol layer (right). (b) SEIRA transmission spectrum T/T_0 of ODT on multilayer nanodisk array with the 1:3 ratios between ZnO and GZO and single-layer GZO nanodisk with 900 nm diameter.

absorptions (2871 and 2957 cm^{-1}) from multilayer nanodisk with 900 nm diameter whose GSP resonance exists at 2700 cm^{-1} (3.7 μm). As shown in Figure 7b, the single-layer GZO nanodisk also enhances the ODT absorption due to its resonance at 4 μm wavelength. This evidence supports the notion that both GSP and LSP resonance are capable of detecting the polymer. However, multilayered configuration can have a wide range of tunability and design of sensing devices with the ability to observe very weak molecular absorption at their resonance and have been able to resolve the presence of nanoscale species.

In conclusion, we studied the plasmonic properties of multilayer TCO nanodisks and observed both localized SPR and GSP inside the dielectric region in the MIM configuration. Additionally, we demonstrated that the resonance wavelengths of a layered structure can be manipulated by varying the thickness ratio of a subwavelength metal and dielectric stack as well as by adjusting the properties of the TCO. We also investigated the performance of GZO/ZnO multilayer nanostructures for SEIRA spectroscopy. We believe that multilayer TCO configurations could pave the way for engineering the optical properties of practical resonant plasmonic device in the IR range and for realizing TCO-based IR devices for biosensing and spectroscopy.

■ ASSOCIATED CONTENT

Supporting Information

Additional supporting figures. The Supporting Information is available free of charge on the ACS Publications website at DOI: 10.1021/acsphotonics.5b00318.

■ AUTHOR INFORMATION

Corresponding Author

*E-mail: aeb@purdue.edu.

Notes

The authors declare no competing financial interest.

■ ACKNOWLEDGMENTS

This work is supported by the U.S. Office of Naval Research Multidisciplinary University Research Initiatives (MURI) program Grant No. ONR-N00014-10-1-0942. We thank Professor Oana Malis for allowing the use of FTIR in her lab and also thank Changhwan Han for useful discussions on STEM characterization.

■ REFERENCES

(1) Maier, S. A. *Plasmonics: Fundamentals and Applications*; Springer Science and Business Media: New York, 2007.

(2) Liu, N.; Tang, M. L.; Hentschel, M.; Giessen, H.; Alivisatos, A. P. Nanoantenna-enhanced gas sensing in a single tailored nanofocus. *Nat. Mater.* **2011**, *10*, 631−636.

(3) Larsson, E. M.; Langhammer, C.; Zorić, I.; Kasemo, B. Nanoplasmonic probes of catalytic reactions. *Science* **2009**, *326*, 1091−1094.

(4) Elghanian, R.; Storhoff, J. J.; Mucic, R. C.; Letsinger, R. L.; Mirkin, C. A. Selective colorimetric detection of polynucleotides based on the distance-dependent optical properties of gold nanoparticles. *Science* **1997**, *277*, 1078−1081.

(5) Moskovits, M. Surface-enhanced spectroscopy. *Rev. Mod. Phys.* **1985**, *57*, 783.

(6) Le, F.; Brandl, D. W.; Urzhumov, Y. A.; Wang, H.; Kundu, J.; Halas, N. J.; Aizpurua, J.; Nordlander, P. Metallic nanoparticle arrays: a common substrate for both surface-enhanced Raman scattering and surface-enhanced infrared absorption. *ACS Nano* **2008**, *2*, 707−718.

(7) Willets, K. A.; Van Duyne, R. P. Localized surface plasmon resonance spectroscopy and sensing. *Annu. Rev. Phys. Chem.* **2007**, *58*, 267−297.

(8) Engheta, N. Circuits with light at nanoscales: optical nanocircuits inspired by metamaterials. *Science* **2007**, *317*, 1698−1702.

(9) Brongersma, M. L.; Shalaev, V. M. The Case for Plasmonics. *Science* **2010**, *328*, 440−441.

(10) Cai, W.; Shalaev, V. M. *Optical Metamaterials*; Springer: New York, 2010; Vol. *10*.

(11) Lal, S.; Link, S.; Halas, N. J. Nano-optics from sensing to waveguiding. *Nat. Photonics* **2007**, *1*, 641−648.

(12) West, P. R.; Ishii, S.; Naik, G. V.; Emani, N. K.; Shalaev, V. M.; Boltasseva, A. Searching for better plasmonic materials. *Laser Photonics Rev.* **2010**, *4*, 795−808.

(13) Blaber, M.; Arnold, M.; Ford, M. Optical properties of intermetallic compounds from first principles calculations: a search for the ideal plasmonic material. *J. Phys.: Condens. Matter* **2009**, *21*, 144211.

(14) Khurgin, J. B.; Boltasseva, A. Reflecting upon the losses in plasmonics and metamaterials. *MRS Bull.* **2012**, *37*, 768−779.

(15) Boltasseva, A.; Atwater, H. A. Low-Loss Plasmonic Metamaterials. *Science* **2011**, *331*, 290−291.

(16) Maradudin, A. A.; Sambles, J. R.; Barnes, W. L. *Modern Plasmonics*; Elsevier: New York, 2014; Vol. *4*.

(17) Bobb, D.; Zhu, G.; Mayy, M.; Gavrilenko, A.; Mead, P.; Gavrilenko, V.; Noginov, M. Engineering of low-loss metal for nanoplasmonic and metamaterials applications. *Appl. Phys. Lett.* **2009**, *95*, 151102.

(18) Naik, G. V.; Shalaev, V. M.; Boltasseva, A. Alternative plasmonic materials: beyond gold and silver. *Adv. Mater.* **2013**, *25*, 3264−3294.

(19) Kim, J.; Naik, G. V.; Gavrilenko, A. V.; Dondapati, K.; Gavrilenko, V. I.; Prokes, S.; Glembocki, O. J.; Shalaev, V. M.; Boltasseva, A. Optical Properties of Gallium-Doped Zinc Oxide—A

DOI: 10.1021/acsphotonics.5b00318
ACS Photonics 2015, 2, 1224−1230

Low-Loss Plasmonic Material: First-Principles Theory and Experiment. *Phys. Rev. X* **2013**, *3*, 041037.
(20) Garcia, G.; Buonsanti, R.; Runnerstrom, E. L.; Mendelsberg, R. J.; Llordes, A.; Anders, A.; Richardson, T. J.; Milliron, D. J. Dynamically modulating the surface plasmon resonance of doped semiconductor nanocrystals. *Nano Lett.* **2011**, *11*, 4415−4420.
(21) Kanehara, M.; Koike, H.; Yoshinaga, T.; Teranishi, T. Indium tin oxide nanoparticles with compositionally tunable surface plasmon resonance frequencies in the near-IR region. *J. Am. Chem. Soc.* **2009**, *131*, 17736−17737.
(22) Diroll, B. T.; Gordon, T. R.; Gaulding, E. A.; Klein, D. R.; Paik, T.; Yun, H. J.; Goodwin, E.; Damodhar, D.; Kagan, C. R.; Murray, C. B. Synthesis of N-Type Plasmonic Oxide Nanocrystals and the Optical and Electrical Characterization of their Transparent Conducting Films. *Chem. Mater.* **2014**, *26*, 4579−4588.
(23) Gordon, T. R.; Paik, T.; Klein, D. R.; Naik, G. V.; Caglayan, H.; Boltasseva, A.; Murray, C. B. Shape-dependent plasmonic response and directed self-assembly in a new semiconductor building block, indium-doped cadmium oxide (ICO). *Nano Lett.* **2013**, *13*, 2857−2863.
(24) Li, S. Q.; Guo, P.; Zhang, L.; Zhou, W.; Odom, T. W.; Seideman, T.; Ketterson, J. B.; Chang, R. P. Infrared plasmonics with indium−tin-oxide nanorod arrays. *ACS Nano* **2011**, *5*, 9161−9170.
(25) Li, S.-Q.; Guo, P.; Buchholz, D. B.; Zhou, W.; Hua, Y.; Odom, T. W.; Ketterson, J.; Ocola, L. E.; Sakoda, K.; Chang, R. P. Plasmonic−photonic mode coupling in indium-tin-oxide nanorod arrays. *ACS Photonics* **2014**, *1*, 163−172.
(26) Jongbum, K.; Naik, G. V.; Emani, N. K.; Guler, U.; Boltasseva, A. Plasmonic Resonances in Nanostructured Transparent Conducting Oxide Films. *IEEE J. Sel. Top. Quantum Electron.* **2013**, *19*, 4601907−4601907.
(27) Abb, M.; Wang, Y.; Papasimakis, N.; de Groot, C.; Muskens, O. L. Surface-Enhanced Infrared Spectroscopy Using Metal Oxide Plasmonic Antenna Arrays. *Nano Lett.* **2014**, *14*, 346−352.
(28) Thomas, D. Infrared absorption in zinc oxide crystals. *J. Phys. Chem. Solids* **1959**, *10*, 47−51.
(29) Naik, G. V.; Kim, J.; Boltasseva, A. Oxides and nitrides as alternative plasmonic materials in the optical range [Invited]. *Opt. Mater. Express* **2011**, *1*, 1090−1099.
(30) Pennycook, S. Z-contrast STEM for materials science. *Ultramicroscopy* **1989**, *30*, 58−69.
(31) Wang, T.; Zalkovskij, M.; Iwaszczuk, K.; Lavrinenko, A. V.; Naik, G. V.; Kim, J.; Boltasseva, A.; Jepsen, P. U. Ultrabroadband terahertz conductivity of highly doped ZnO and ITO. *Opt. Mater. Express* **2015**, *5*, 566−575.
(32) Langhammer, C.; Schwind, M.; Kasemo, B.; Zoric, I. Localized surface plasmon resonances in aluminum nanodisks. *Nano Lett.* **2008**, *8*, 1461−1471.
(33) Langhammer, C.; Yuan, Z.; Zoric, I.; Kasemo, B. Plasmonic properties of supported Pt and Pd nanostructures. *Nano Lett.* **2006**, *6*, 833−838.
(34) Pors, A.; Bozhevolnyi, S. I. Plasmonic metasurfaces for efficient phase control in reflection. *Opt. Express* **2013**, *21*, 27438−27451.
(35) Cai, W.; Chettiar, U. K.; Yuan, H.-K.; de Silva, V. C.; Kildishev, A. V.; Drachev, V. P.; Shalaev, V. M. Metamagnetics with rainbow colors. *Opt. Express* **2007**, *15*, 3333−3341.
(36) Yuan, H.-K.; Chettiar, U. K.; Cai, W.; Kildishev, A. V.; Boltasseva, A.; Drachev, V. P.; Shalaev, V. M. A negative permeability material at red light. *Opt. Express* **2007**, *15*, 1076−1083.
(37) Jung, J.; Søndergaard, T.; Bozhevolnyi, S. I. Gap plasmon-polariton nanoresonators: Scattering enhancement and launching of surface plasmon polaritons. *Phys. Rev. B: Condens. Matter Mater. Phys.* **2009**, *79*, 035401.
(38) Bozhevolnyi, S. I. General properties of slow-plasmon resonant nanostructures: nano-antennas and resonators. *Opt. Express* **2007**, *15*, 10869−10877.
(39) Søndergaard, T.; Jung, J.; Bozhevolnyi, S. I.; Della Valle, G. Theoretical analysis of gold nano-strip gap plasmon resonators. *New J. Phys.* **2008**, *10*, 105008.
(40) Drachev, V. P.; Chettiar, U. K.; Kildishev, A. V.; Yuan, H.-K.; Cai, W.; Shalaev, V. M. The Ag dielectric function in plasmonic metamaterials. *Opt. Express* **2008**, *16*, 1186−1195.
(41) Lin-Vien, D.; Colthup, N. B.; Fateley, W. G.; Grasselli, J. G. *The Handbook of Infrared and Raman Characteristic Frequencies of Organic Molecules*; Elsevier: New York, 1991.
(42) Tarlov, M. J. Silver metalization of octadecanethiol monolayers self-assembled on gold. *Langmuir* **1992**, *8*, 80−89.

DOI: 10.1021/acsphotonics.5b00318
ACS Photonics 2015, 2, 1224−1230